

Cooperative Thermal-Electric Field Control of Infrared Modulation Using a Vanadium Dioxide Film-Based Modulator

Chang Lu, Fan Yang, Min Gao,* Xinzhong Wang, and Yuan Lin*

Cite This: *ACS Omega* 2023, 8, 46399–46405

Read Online

ACCESS |



Metrics & More

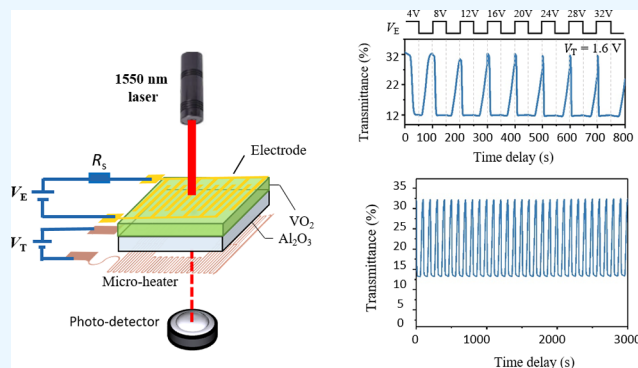


Article Recommendations



Supporting Information

ABSTRACT: Vanadium dioxide (VO_2) has garnered significant attention as a material for actively tunable infrared (IR) modulators due to its reversible and responsive modulation effect on IR radiation, which is accompanied by its intrinsic insulator–metal phase transition (IMT). Here, we propose a multilayer device structure that integrates VO_2 film with microheater and interdigitated electrodes for cooperative thermal-electric field control of IMT. Our results demonstrate that while intense electric fields can trigger abrupt IMT, deep modulation of IR radiation requires energy integration through Joule heating, which limits the response time of IR transmission controlled by electric field. Thus, cooperative thermal-electric field control, which provides a constant, uniform temperature field while electrically switching the IMT, is more effective for achieving a faster response time and retaining the intrinsic modulation depth of VO_2 -based IR modulators. Our findings offer valuable insights for the development of VO_2 -based IR modulators with improved performance.



INTRODUCTION

As a key component of infrared (IR) communication systems, IR modulator has drawn a lot of attention for its applications in signal manipulation.^{1–3} Researchers have made significant efforts to identify new materials that can actively switch IR properties and offer a deep modulation depth (MD). The insulator–metal phase transition (IMT) of vanadium dioxide (VO_2), which is in response to various stimuli and accompanied by dramatic changes in optical properties across at IR frequencies, has been regarded as a promising candidate for IR modulators.^{4,5} However, using VO_2 film as a core component to fabricate IR modulators still faces limitations. A key problem is the critical temperature ($\sim 68^\circ\text{C}$) of the VO_2 film that is well above the room temperature, which restricts the response time when switching VO_2 thermally between the insulating and metallic states.⁶ This phenomenon is due to the first-order phase transition nature of VO_2 film, resulting in an energy barrier that hinders the phase transition.⁷ Minimizing the energy barrier through manipulating the microscopic properties of VO_2 film is an effective approach but is accompanied by unavoidable degradation in MD.^{8,9} Progress has also been made in the control methods for VO_2 films. In addition to fundamental temperature control through heating and cooling cycles, alternative switching methods have also been explored. These methods include electric field manipulation,^{10–14} high-energy laser techniques,^{15,16} and electrochemical modifications.^{17,18} These advanced methods provide

a portable and miniaturized means for implementing built-in active excitation.

Electric field is one of the most researched triggering schemes for VO_2 film due to its potential to be integrated in versatile device structures.^{10–14} The commonly accepted mechanism is thought to involve both Joule heating and nonthermal doping effects within channels, indicating high thermal field and reduced phase transition barrier, respectively.^{19–22} As a result, the response time of IMT triggered by electric field is lower than those managed by a temperature field. However, the electric field threshold of pure VO_2 films is extremely high, ranging from 1.5×10^6 to 2.6×10^6 V/m, depending on ambient temperature, initial resistance, and electrode geometry.²⁰ This high electric field threshold limits the fill area of the VO_2 component, which is critical to the practical application of VO_2 -based IR modulators and requires further research efforts to overcome.

In this study, we propose a multilayer device structure composed of serpentine circuits/ VO_2 /interdigitated electrodes to achieve cooperative thermal-electric field control of IMT.

Received: April 11, 2023

Revised: September 19, 2023

Accepted: October 31, 2023

Published: November 28, 2023



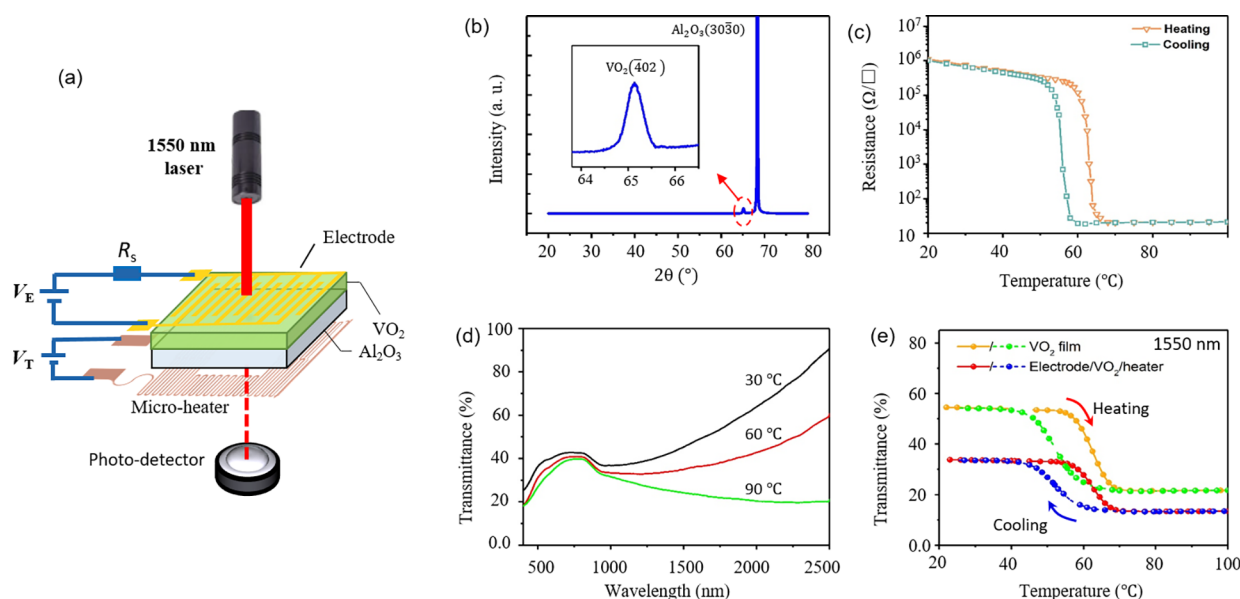


Figure 1. Characterization of VO₂ film. (a) Schematic of the experimental setup used to measure optical modulation by the VO₂ film. (b) XRD pattern of VO₂ film. (c) Temperature-dependent sheet resistance of VO₂ film measured using the 4-probe method. (d) IR transmittance of VO₂ film at 30, 60, and 90 °C. (e) Transmittance of the VO₂ film as a function of temperature at a wavelength of 1550 nm.

The microheater, made of serpentine circuits, is attached to the bottom of the sapphire substrate to provide stable and responsive thermal field control, while the interdigitated electrodes are patterned on the top to actively regulate the electric field inside channels. We demonstrated that by maintaining the VO₂ film in the vicinity of phase transition thermally and switching the IMT electrically, significant improvements in response time are achieved while the intrinsic MD of the VO₂ film could be retained, which is crucial for the further development of VO₂-based IR switchers.

EXPERIMENTAL SECTION

The polymer-assisted deposition method was utilized to fabricate VO₂ films on (10 $\bar{1}$ 0) sapphire substrate.²³ A precursor solution containing vanadium ions was prepared by dissolving 3 g of polyethylenimine and 3 g of ethylenediaminetetraacetic acid in 50 mL of deionized water. This solution was mixed with 1.2 g of ammonium metavanadate (NH₄VO₃) dissolved in 30 mL of deionized water, and the NH₄⁺ ions were removed via an Amicon filtration process. The precursor solution was then spin-coated on the sapphire substrate using a low speed of 500 rpm for 10 s, followed by a high speed of 7000 rpm for 40 s. The precursor films were then thermally treated at a rate of 0.8 °C/min to reach a temperature of 450 °C and held at this temperature for 120 min to decompose the polymer. Subsequently, the films were annealed at 505 °C for 120 min to crystallize the film. The heating process employed a balanced environment created by forming gas (98.5% N₂ + 1.5% H₂) and moisture to achieve a proper equilibrium oxygen partial pressure. The film thickness was analyzed using scanning electron microscopy (Figure S1, Supporting Information).

RESULTS AND DISCUSSION

Figure 1a illustrates the modulator structure designed for multistimulus control of IR transmittance. We utilized an IR laser (1.2 mW, Alphanov) with a vertical incidence and a 3 mm spot size for the transmittance (1550 nm) experiments. The

transmitted laser power was measured using a photodiode (Thorlabs PM200) detector. To enable thermal field control, a serpentine-shaped microheater with a 100 μm line width was attached to the backside of the sapphire substrate, and the voltage applied to the microheater was denoted as V_T. The transmission window was designed to minimize the heater circuit's inversion loss and was approximately 3 mm in size. Interdigitated electrodes with a finger width of 100 μm and a finger spacing of 100 μm were deposited on the VO₂ film to facilitate electric control, and the applied voltage was noted as V_E. To protect against overcurrent in the case of a metalized VO₂ gap, a current-limiting resistor (R_s) was used. Nano-second laser cutting technology was used to fabricate both the microheater and interdigitated electrode. A copper tape was used to create the microheater through a cutting and transferring sequence, while a gold film was used to create the parallel electrodes through a laser-cut mask and sputtering deposition method to optimize the contact between VO₂ and the electrodes. In Figure S1 (Supporting Information), we demonstrate the control of the microheater and parallel electrode using a two-channel signal generator. This setup allows for the simultaneous control of the temperature field and electrical switching, providing the potential for thermal, electric, and cooperative thermal-electric-induced IMT in this modulator.

The proposed VO₂-based modulator exhibits a significant modulation of IR radiation (1550 nm) across the IMT. The high-resolution X-ray diffraction (XRD) pattern presented in Figure 1b shows a single peak of the VO₂ film at 65.10°, demonstrating the epitaxial growth of VO₂ crystallites with (402) orientation. Temperature-dependent measurements of the film sheet resistance in Figure 1c confirm the high quality of the VO₂ film's IMT, revealing a sharp change over 4 orders of magnitude. Figure 1d illustrates the IR transmittance spectroscopy of the as-prepared VO₂ film across the IMT, as measured by a PE Lambda950. This spectroscopy demonstrates the significant modulation effect of the VO₂ film on the IR wavelength. Figure 1e presents a more detailed analysis of

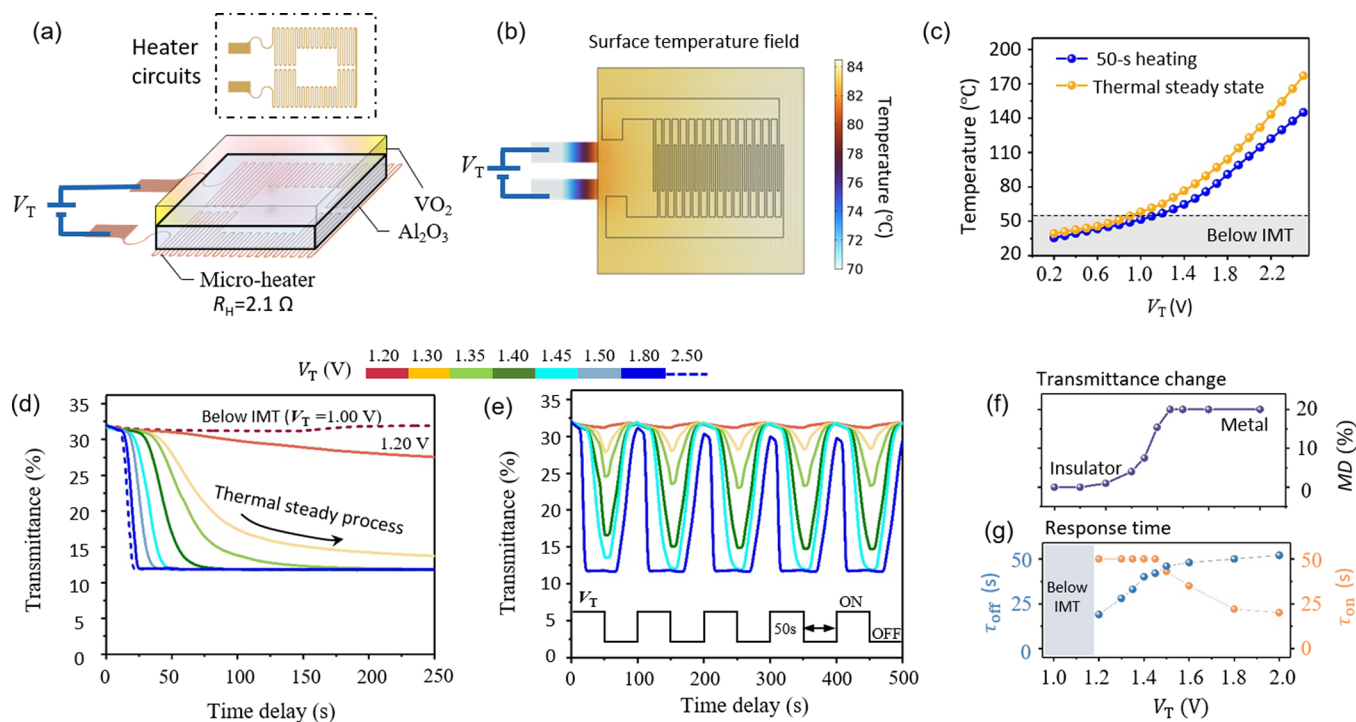


Figure 2. Modulation of transmission using thermal field-driven control. (a) Schematic illustrating the setup of heater circuit. (b) Simulation of surface temperature distribution with $V_T = 1.8$ V. (c) Surface temperature as a function of applied V_T measured by IR images. (d) Time-delay dependent IR transmittance in response to switching-on of V_T . (e) Timing diagrams of transmission monitored by periodic V_T signal (50 s on and off). (f) MD as a function of applied V_T (50 s on and off). (g) Responding times τ_{on} and τ_{off} as a function of applied V_T .

the transmittance at 1550 nm, measured as the transmitted laser power normalized to the incident laser power. The transmittance measurements were conducted for both the bare VO_2 film and the structured serpentine-circuit/ VO_2 /interdigitated-electrode configuration with temperature control facilitated by a thermal stage. The transmittance of the bare VO_2 film was observed to change from 53.6 to 21.6%. In contrast, the structured VO_2 -based modulator, incorporating interdigitated electrodes, exhibited a decrease in IR transmittance of the VO_2 film, resulting in a transmittance change from 33.1 to 13.6%. Consequently, the MD of the modulator across the IMT (defined as $\text{MD} = T_{\text{Low}} - T_{\text{High}}$, where T_{Low} and T_{High} are the transmittance at low and high temperatures, respectively) is approximately 19.5%. While the electrode may reduce the overall transmittance of the sample, it is essential to note that the aspect ratio of IR light before and after the IMT remains relatively unchanged. This characteristic renders our proposed device structure well-suited for applications in environments where exceptionally high light transmittance is not a critical requirement, such as laser protection.²⁴ Additionally, the utilization of precision fabrication processes to optimize the electrode structure, potentially involving the reduction of the electrode coverage ratio, holds promise for further enhancement of light transmittance.

The thermal field control of IR transmission in Figure 2a uses a serpentine circuit (shown in inset) to trigger the IMT. This process can be modeled by the thermodynamic equation:

$$P_{\text{in}} = G_E(T - T_E) + (C_{\text{sub}} + C_{\text{film}}) \frac{dT}{dt} \quad (1)$$

where P_{in} is the power dissipation ($P_{\text{in}} = V_T^2/R_{\text{Heater}}$ in microheater control scheme), T is the temperature of the VO_2 film and substrate, t is the time delay, G_E and T_E denote the

heat conductance and temperature of environment, C_{sub} and C_{film} are the thermal capacitances of the sapphire substrate and VO_2 film, respectively. Thus, it can be concluded that as P_{in} accumulates and the temperature increases, the heat energy conducted to the environment increases, pushing the temperature of the VO_2 film to a steady state. By utilizing the provided equation, finite element analysis was performed, resulting in a balanced interplay between Ohm heating and energy conduction. This equilibrium led to the creation of a uniform temperature field, as shown in Figure 2b. The microheater was subjected to a 1.8 V voltage, and the temperature variation observed on the surface was approximately within ~ 4 °C. This simulation is only used to demonstrate a uniform temperature field on the surface. To determine the actual relationship between V_T and surface temperature, IR images were captured and analyzed, as depicted in Figure S3 of the Supporting Information. For accurate measurements, a reference sample without a VO_2 layer was employed, as the variable emissivity of the VO_2 film during the IMT could introduce uncertainties in the measurements. Both the temperatures after 50 s annealing and at thermal steady state are provided as a function of V_T in Figure 2c.

Figure 2d exhibits the IR transmission in response to constant V_T , illustrating a thermally steady process leading up to the final MD. It is evident that when V_T is below 1.0 V, the VO_2 film remains in the insulating state, resulting in negligible changes in the IR transmittance. However, as V_T increases from 1.2 to 1.8 V, the modulation effect on IR transmittance gradually intensifies, with the MD increasing from MD = 4% to MD = 19.5%. We have expanded the voltage range of V_T from 1.8 to 2.5 V in Figure 2d. In contrast to the case of $V_T = 1.8$ V, a slightly faster response time was achieved by increasing V_T to

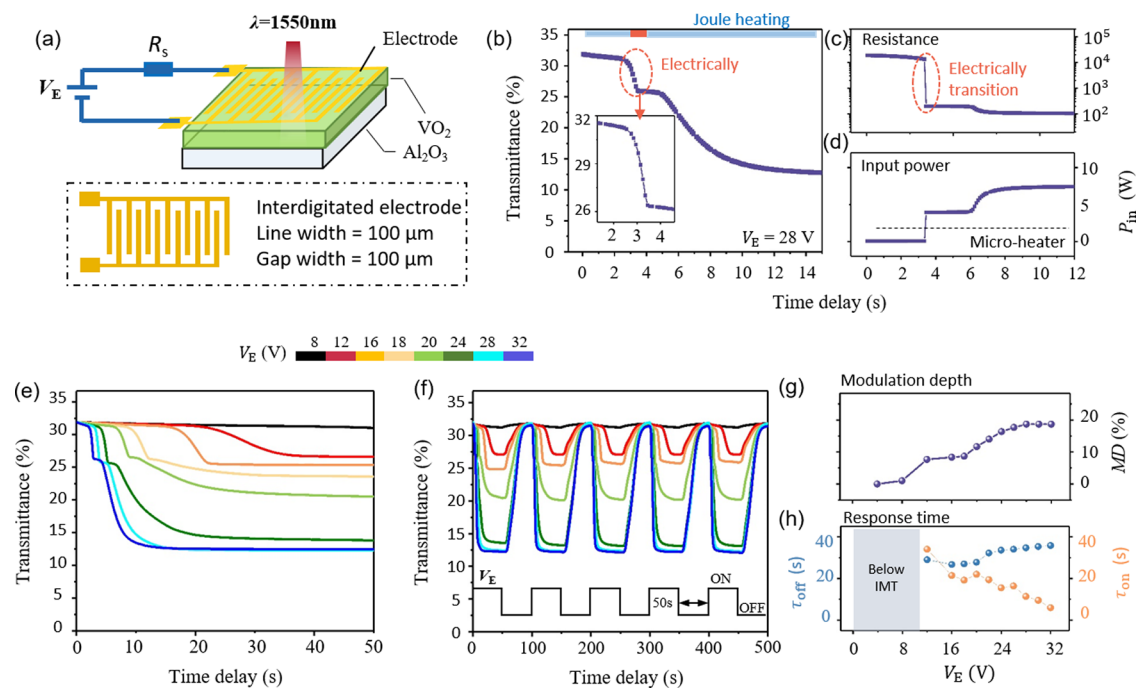


Figure 3. Modulation of transmission using electric field-driven control. (a) Schematic diagram of the interdigital electrode used for electric field modulation. (b) Time-dependent transmission profile. (c) Resistance of the VO_2 gap and current through the electrode. (d) Input power as a function of voltage applied to the interdigital electrode ($V_E = 28\ \text{V}$). (e) Transmission as a function of time delay under a constant V_E . (f) Timing diagrams of transmission monitored by a periodic V_E signal (50 s on and 50 s off). (g) MD as a function of applied V_E (50 s on and 50 s off). (h) Response time (τ_{on}) as a function of the applied V_E .

2.5 V, resulting in a reduction of approximately 3 s. However, it is important to note that for V_T approaching 2.5 V, the temperature of the VO_2 film can exceed $150\ ^\circ\text{C}$. This high temperature can cause oxidation of the VO_2 film when exposed to air. To ensure the stability and integrity of the VO_2 film, we chose to limit the voltage applied to the heater to below 1.8 V.

Additionally, we monitored periodic transmission waveforms in Figure 2e, which were triggered by a periodic V_T signal (50 s on and off). The MD of this control scheme is related to the value of V_T , as summarized in Figure 2f. The time it takes for IR transmission to fall to 90% of its maximum value in response to the switching-on of V_T is denoted as τ_{on} , while the rising time of IR transmission reaching 90% of the room-temperature transmission in response to the switching-off of V_T is represented as τ_{off} . The relationship between V_T and $\tau_{\text{on}}/\tau_{\text{off}}$ is summarized in Figure 2g. It was observed that while increasing V_T and enlarging the power dissipation can decrease τ_{on} , τ_{off} of the modulator is nearly independent of V_T . Additionally, it can be seen that the decreasing trend of τ_{on} slows down above $V_T = 1.8\ \text{V}$, indicating that the improvement in response time caused by increasing V_T has limitations.

The electric field control of IR transmission shown in Figure 3a involves the utilization of interdigital electrode and a series resistor ($R_s = 100\ \Omega$) for current limiting. In response to the switching-on of V_E (28 V), the timing transmission diagram in Figure 3b displays a step profile. To explain this phenomenon, we measured the current passing through the electrode and calculated the resistance of the VO_2 gap (R_{VO_2}), as shown in Figure 3c. We found that although the resistance of the VO_2 gap dropped significantly at approximately 3.0 s, indicating that the intense electric field triggered IMT, it still took seconds for the modulator to reach its maximum MD.

To determine the presence of an electric field-driven IMT, we conducted simulations to analyze the strength of the electric field generated by the $100\ \mu\text{m}$ spaced interdigital electrodes (Figure S4, Supporting Information). The simulation results reveal an electric field strength of approximately $2.7 \times 10^5\ \text{V/m}$. Although this value is smaller than the reported threshold electric field strength ($2 \times 10^6\ \text{V/m}$) for electrically driven IMT at room temperature, it falls within the range of electrically driven IMT observed at temperatures near the phase transition temperature (at around $50\ ^\circ\text{C}$).^{14,25} Previous research has demonstrated that during the IMT driven by a DC electric field, Joule heating assumes a predominant role.²⁰ Initially, the flow of DC current leads to Joule heating, resulting in the formation of larger metallic domains and eventually creating a conductive path within the insulating background.^{26,27} This mechanism elucidates the observed two-step process illustrated in Figure 3b: First, the current flow heats the VO_2 layer, resulting in a slight decrease in IR transmittance. Subsequently, larger VO_2 domains form, leading to a sharp decrease in transmittance. Finally, as Joule heating accumulates, it fully metalizes the VO_2 layer, ultimately resulting in saturation of the modulation effect.

In Figure 3d, we calculated the P_{in} ($P_{\text{in}} = V_E^2/R_{\text{VO}_2}$) applied through the interdigital electrode. Initially, the interdigital electrode exhibited low P_{in} due to the high value of R_{VO_2} below IMT, and P_{in} increases rapidly after R_{VO_2} decreased due to IMT. The dashed line in Figure 3d shows the P_{in} for microheater control with $V_T = 1.8\ \text{V}$, providing a comparison of power dissipation between thermal field control and electric field control. The P_{in} of electric field control changes from being smaller than to much larger than the P_{in} of thermal control as the IMT is triggered, resulting in a faster τ_{on} ($\sim 9.8\ \text{s}$) compared with the τ_{on} ($\sim 21.5\ \text{s}$) of thermal field control.

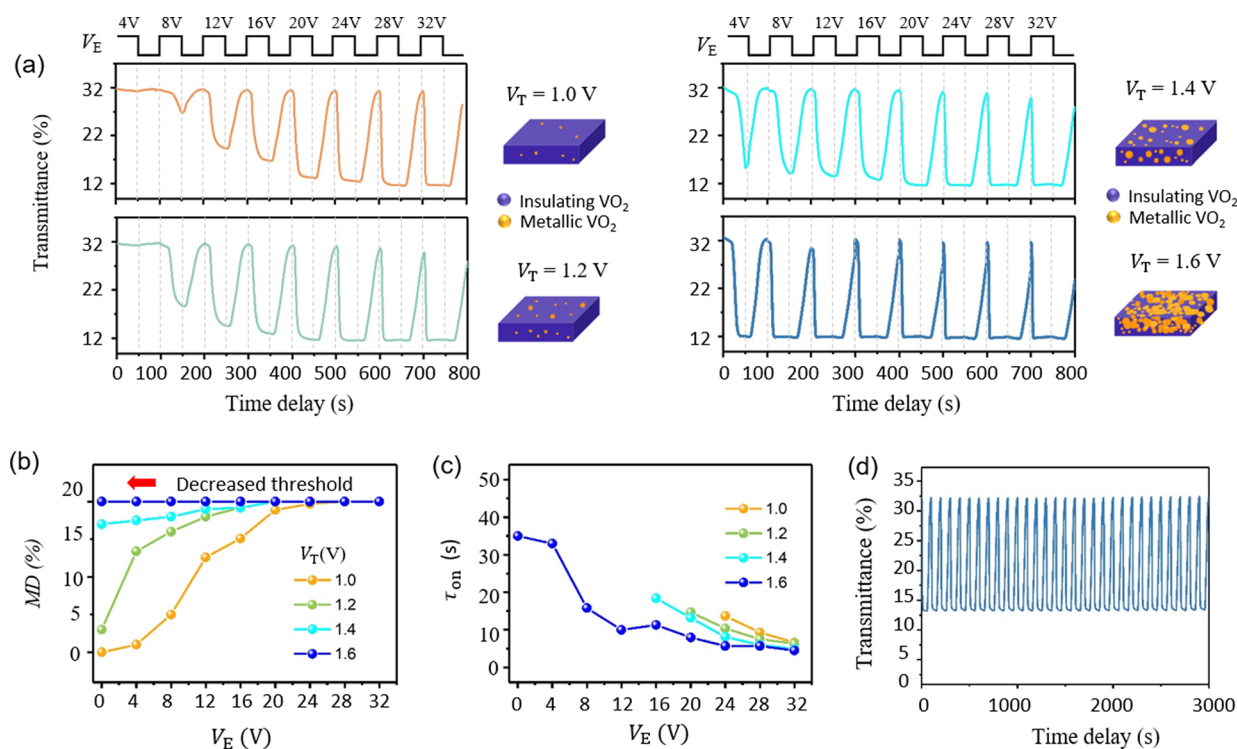


Figure 4. Modulation of transmission using cooperative thermal-electric field-driven control. (a) Timing diagrams of transmission monitored by periodic V_E (increased from 4 to 32 V) and periodic V_T (both 50 s on and off). (b) MD as a function of applied V_E and V_T . (c) Response time (τ_{on}) as a function of the applied V_E and V_T . (d) Timing diagrams of transmission monitored by multicycles control signals ($V_T = 1.4$ V, $V_E = 28$ V).

However, IMT triggered by an electric field is accompanied by a high threshold voltage. The time-dependent transmission in Figure 3e reveals that V_E below 8.0 V cannot trigger IMT, while V_E ranging from 8 to 24 V partially triggers IMT and results in unsaturated MD. The threshold voltage for a fully metalized VO_2 film is 28 V, above which a saturation MD of $\sim 20\%$ is achieved. Figure 3f displays the monitored transmission diagram controlled by the periodic V_E signal (50 s on and off), and the MD and response time in this control scheme are summarized in Figure 3g,h, respectively. As V_E increases, the MD of the modulator increases and reaches saturation as V_E approaches 28 V. While the τ_{on} in response to switching-on of V_E is observed to decrease with increasing V_E , the τ_{off} remains independent of V_E . The response time τ_{on} for electric field control is much shorter compared to the modulation controlled by a microheater.

We have demonstrated that the modulation of IR transmission triggered by an electric field results from a combination of electrically induced IMT and the accumulated thermal effect of Joule heating. These findings suggest that it may be possible to reduce the response time τ_{on} and lower the threshold voltage of electric field control by cooperating thermal field control with electric field control. Figure 4a displays the monitored timing transmission diagram results of applying V_E and V_T simultaneously. In this control scheme, V_T remains constant while V_E is increased from 4 to 32 V in steps of 4 V (both V_T and V_E in 50 s on and off cycles). The MD of this control scheme is summarized in Figure 4b. We observe that when V_T is 1.0 V, the constant temperature of the VO_2 film is maintained below IMT by a microheater, and the threshold V_E for saturation MD is 24 V, similar to that of zero V_T . While for $V_T = 1.2$ V, thermal field through the microheater maintains the VO_2 film at an early stage of

IMT, where small volumes of metallic phase have been formed, decreasing the threshold V_E for saturation MD from 32 to 20 V. As V_T approaches 1.4 V, the threshold V_E is decreased to 16 V. However, with $V_T = 1.4$ V and $V_E = 32$ V, we observe that the VO_2 film cannot recover to the insulating state after several cycles of heating and cooling, resulting in decreased MD. This phenomenon is due to the accumulation of heat energy that is not conducted to the environment, resulting in increased recovery time after multiple cycles (Section 5, Supporting Information). Hence, to ensure prolonged operation, it is advisable to restrict the value of V_E to no greater than 28 V. Furthermore, we have observed that the response speed improves when V_E and V_T are applied simultaneously. This effect is demonstrated in Figure 4c, where the response time τ_{on} under various V_E and V_T conditions is summarized (only the saturation state is analyzed). In comparison to the optimal τ_{on} of 9.8 s for single electric field control, employing cooperative thermal-electric field control reduces the τ_{on} to approximately 4.9 s. Figure 4d presents timing diagrams, showcasing the transmission monitored by multicycle control signals ($V_T = 1.4$ V, $V_E = 28$ V) and illustrating the capability of the designed IR modulator to operate across multiple cycles.

The comparison of switching time and working voltage among different triggering schemes, including the thermal field, electric field, and cooperative thermal-electric field, highlights the unique characteristics of each approach. The thermal field control method, which employs a microheater, has a slower response time due to the thermal steady-state process. In contrast, the electric field control method, which uses an interdigital electrode, allows for abrupt electrical switching and confines the thermal effect of Joule heating to the electrode channels, resulting in a longer response time. The cooperative thermal-electric field approach further improves the response

time by maintaining a constant thermal field and triggering the IMT electrically. This approach softens the energy barrier of IMT by using the thermal field and leverages the fast response time of electrical triggering. Additionally, the complementary effect of thermal and electric fields on the IMT provides a flexible option for controlling the IMT by manipulating the aspect ratio of the fields, offering a compromise between response time and threshold voltage.

CONCLUSIONS

In summary, we have demonstrated an IR switch using a multilayer structure composed of serpentine circuits/ VO_2 /interdigitated electrodes. By using the cooperative thermal-electric field-driven phase transition of the VO_2 film, we achieved a MD of up to $\sim 20\%$ in just ~ 4.9 s. This response time is significantly faster than the ~ 21.5 and ~ 9.8 s response times achieved through thermal control and electric field control, respectively. The improvement can be attributed to the complementary effect of thermal and electric fields on IMT, allowing for the maintenance of VO_2 in the vicinity of IMT while simultaneously switching the IMT electrically. Our research not only highlights the advantages of cooperative thermal-electric field stimulation but also presents a simple and scalable device construction for large-area IR switchers.

ASSOCIATED CONTENT

Supporting Information

The Supporting Information is available free of charge at <https://pubs.acs.org/doi/10.1021/acsomega.3c02469>.

Experiment setup for comparative thermal-electric field control; film thickness measured by scanning electron microscopy; surface temperature detected by infrared image; electric field distribution within VO_2 film; and recovering time of IR modulation under simultaneous control of V_E and V_T (PDF)

AUTHOR INFORMATION

Corresponding Authors

Min Gao – School of Materials and Energy, University of Electronic Science and Technology of China, Chengdu 610054, China; orcid.org/0000-0003-3899-2933; Email: mingao@uestc.edu.cn

Yuan Lin – School of Materials and Energy, University of Electronic Science and Technology of China, Chengdu 610054, China; Engineering Cooperation on Applied Medicine Research Center, University of Electronic Science and Technology of China, Chengdu 610054, China; Email: linyin@uestc.edu.cn

Authors

Chang Lu – Department of Electronic Communication and Technology, Shenzhen Institute of Information Technology, Shenzhen 518029, China; School of Materials and Energy, University of Electronic Science and Technology of China, Chengdu 610054, China; orcid.org/0000-0003-1353-0118

Fan Yang – School of Materials and Energy, University of Electronic Science and Technology of China, Chengdu 610054, China

Xinzhong Wang – Department of Electronic Communication and Technology, Shenzhen Institute of Information Technology, Shenzhen 518029, China

Complete contact information is available at:

<https://pubs.acs.org/10.1021/acsomega.3c02469>

Author Contributions

Y.L., M.G., and C.L. conceived research. C.L. and F.Y. fabricated the devices and did all the measurements. C.L. and M.G. cowrote the paper. Y.L. and M.G. supervised the research. All authors discussed the results and commented on the manuscript.

Notes

The authors declare no competing financial interest.

ACKNOWLEDGMENTS

This work is supported by the Natural Science Foundation of China (Nos. 52272138, 61825102, U21A20460, and 52021001), and the Science and Technology Plan of Sichuan Province of China (No. 2022ZHCG0041).

REFERENCES

- Herrmann, E.; Gao, H.; Huang, Z. X.; Sitaram, S. R.; Ma, K.; Wang, X., Modulators for mid-infrared and terahertz light. *J. Appl. Phys.* **2020**, *128* (14), 140903, DOI: [10.1063/5.0025032](https://doi.org/10.1063/5.0025032)
- Montesinos-Ballester, M.; Deniel, L.; Koumpai, N.; Nguyen, T. H. N.; Frigerio, J.; Ballabio, A.; Falcone, V.; Le Roux, X.; Alonso-Ramos, C.; Vivien, L.; Bousseksou, A.; Isella, G.; Marris-Morini, D. Mid-infrared Integrated Electro-optic Modulator Operating up to 225 MHz between 6.4 and 10.7 μm Wavelength. *ACS Photonics* **2022**, *9* (1), 249–255.
- Georgiev, G. V.; Cao, W.; Zhang, W. W.; Ke, L.; Thomson, D. J.; Reed, G. T.; Nedeljkovic, M.; Mashanovich, G. Z., Near-IR & Mid-IR Silicon Photonics Modulators. *Sensors* **2022**, *22* (24), 9620, DOI: [10.3390/s22249620](https://doi.org/10.3390/s22249620)
- Ke, Y. J.; Wang, S. C.; Liu, G. W.; Li, M.; White, T. J.; Long, Y., Vanadium Dioxide: The Multistimuli Responsive Material and Its Applications. *Small* **2018**, *14* (39), e1802025, DOI: [10.1002/sml.201802025](https://doi.org/10.1002/sml.201802025)
- Cui, Y. Y.; Ke, Y. J.; Liu, C.; Chen, Z.; Wang, N.; Zhang, L. M.; Zhou, Y.; Wang, S. C.; Gao, Y. F.; Long, Y. Thermo-chromic VO_2 for Energy-Efficient Smart Windows. *Joule* **2018**, *2* (9), 1707–1746.
- Shao, Z. W.; Cao, X.; Luo, H. J.; Jin, P. Recent progress in the phase-transition mechanism and modulation of vanadium dioxide materials. *NPG Asia Mater.* **2018**, *10*, 581.
- Liu, K.; Lee, S.; Yang, S.; Delaire, O.; Wu, J. Q. Recent progresses on physics and applications of vanadium dioxide. *Mater. Today* **2018**, *21* (8), 875–896.
- Hiroi, Z. Structural instability of the rutile compounds and its relevance to the metal-insulator transition of VO_2 . *Prog. Solid State Chem.* **2015**, *43* (1–2), 47–69.
- Liu, D. Q.; Cheng, H. F.; Xing, X.; Zhang, C. Y.; Zheng, W. W. Thermo-chromic properties of W-doped VO_2 thin films deposited by aqueous sol-gel method for adaptive infrared stealth application. *Infrared Phys. Technol.* **2016**, *77*, 339–343.
- Cai, H. L.; Chen, S.; Zou, C. W.; Huang, Q. P.; Liu, Y.; Hu, X.; Fu, Z. P.; Zhao, Y.; He, H. C.; Lu, Y. L., Multifunctional Hybrid Metasurfaces for Dynamic Tuning of Terahertz Waves. *Adv. Opt. Mater.* **2018**, *6* (14), 1800257, DOI: [10.1002/adom.201800257](https://doi.org/10.1002/adom.201800257)
- Kim, Y.; Wu, P. C.; Sokhoyan, R.; Mauser, K.; Glauddell, R.; Shirmanesh, G. K.; Atwater, H. A. Phase Modulation with Electrically Tunable Vanadium Dioxide Phase-Change Metasurfaces. *Nano Lett.* **2019**, *19* (6), 3961–3968.
- Markov, P.; Marvel, R. E.; Conley, H. J.; Miller, K. J.; Haglund, R. F.; Weiss, S. M. Optically Monitored Electrical Switching in VO_2 . *ACS Photonics* **2015**, *2* (8), 1175–1182.
- Bayram, F.; Gajula, D.; Uppalapati, B.; Khan, D.; Koley, G. Electrical Modulation Transmitted Ir Light through VO_2 Thin Film on Gan Membranes. In *International Conference on Solid-State Sensors, Actuators and Microsystems*; **2021**; pp 593–596.

(14) Bayram, F.; Gajula, D.; Khan, D.; Uppalapati, B.; Azad, S.; Koley, G. Voltage triggered near-infrared light modulation using VO₂ thin film. *Opt. Express* **2021**, *29* (20), 32124–32134.

(15) Wegkamp, D.; Stahler, J. Ultrafast dynamics during the photoinduced phase transition in VO₂. *Prog. Surf. Sci.* **2015**, *90* (4), 464–502.

(16) Fu, W.; Ma, H.; Wei, Y.; Jiang, K. L.; Fei, G. T.; Zhang, L. D. Preparation and infrared response properties of vanadium dioxide nanowire/carbon nanotube composite film. *J. Mater. Sci.* **2017**, *52* (12), 7224–7231.

(17) Nakano, M.; Shibuya, K.; Okuyama, D.; Hatano, T.; Ono, S.; Kawasaki, M.; Iwasa, Y.; Tokura, Y. Collective bulk carrier delocalization driven by electrostatic surface charge accumulation. *Nature* **2012**, *487* (7408), 459–462.

(18) Deng, X.; Zhao, Y. F.; Zhong, N.; Yue, F. Y.; Huang, R.; Peng, H.; Tang, X. D.; Xiang, P. H.; Chu, Y. H.; Duan, C. G. Proton-Mediated Phase Control in Flexible and Transparent Mott Transistors. *Adv. Electron. Mater.* **2020**, *6* (1), No. 1900742.

(19) Kalcheim, Y.; Camjayi, A.; del Valle, J.; Salev, P.; Rozenberg, M.; Schuller, I. K. Non-thermal resistive switching in Mott insulator nanowires. *Nat. Commun.* **2020**, *11*, 2985.

(20) Zimmers, A.; Aigouy, L.; Mortier, M.; Sharoni, A.; Wang, S. M.; West, K. G.; Ramirez, J. G.; Schuller, I. K. Role of Thermal Heating on the Voltage Induced Insulator-Metal Transition in VO₂. *Phys. Rev. Lett.* **2013**, *110* (5), 056601, DOI: 10.1103/PhysRevLett.110.056601

(21) Shabalin, A. G.; del Valle, J.; Hua, N.; Cherukara, M. J.; Holt, M. V.; Schuller, I. K.; Shpyrko, O. G. Nanoscale Imaging and Control of Volatile and Non-Volatile Resistive Switching in VO₂. *Small* **2020**, *16* (50), 5439.

(22) Valmianski, I.; Wang, P. Y.; Wang, S.; Ramirez, J. G.; Guenon, S.; Schuller, I. K. Origin of the current-driven breakdown in vanadium oxides: Thermal versus electronic. *Phys. Rev. B* **2018**, *98* (19), No. 195144.

(23) Liang, W. Z.; Gao, M.; Lu, C.; Zhang, Z.; Chan, C. H.; Zhuge, L. J.; Dai, J. Y.; Yang, H.; Chen, C. L.; Park, B. H.; Jia, Q.; Lin, Y. Enhanced Metal-Insulator Transition Performance in Scalable Vanadium Dioxide Thin Films Prepared Using a Moisture-Assisted Chemical Solution Approach. *ACS Appl. Mater. Interfaces* **2018**, *10* (9), 8341–8348.

(24) Chen, S. H.; Ma, H.; Yi, X. J.; Xiong, T.; Wang, H. C.; Ke, C. J. Smart VO₂ thin film for protection of sensitive infrared detectors from strong laser radiation. *Sens. Actuators, A* **2004**, *115* (1), 28–31.

(25) Tadjer, M. J.; Wheeler, V. D.; Downey, B. P.; Robinson, Z. R.; Meyer, D. J.; Eddy, C. R.; Kub, F. J. Temperature and electric field induced metal-insulator transition in atomic layer deposited VO₂ thin films. *Solid-State Electron.* **2017**, *136*, 30–35.

(26) Manousou, D. K.; Gardelis, S.; Calamiotou, M.; Likodimos, V.; Syskakis, E., Two-step current-temperature-induced electrical and optical modifications in VO₂ films around the metal-insulator transition. *J. Appl. Phys.* **2021**, *130* (4), 045107, DOI: 10.1063/5.0052954

(27) Kumar, S.; Pickett, M. D.; Strachan, J. P.; Gibson, G.; Nishi, Y.; Williams, R. S. Local Temperature Redistribution and Structural Transition During Joule-Heating-Driven Conductance Switching in VO₂. *Adv. Mater.* **2013**, *25* (42), 6128–6132.